Advanced Engineering & Precision Manufacturing
WISDOM ACADEMIC ISSN: 3105-1693 | E-ISSN: 3105-1707 *Volume 2 , Issue 1*

Article

The propeller design of a grazing drone based on MATLAB and XFOIL to select the optimal foil cross-section airfoil

Chenyang Guan[1], Xiaojun Ma[2], Bing Guo[1,*]

[1]School of Mechanical Engineering, Qinghai University, Xining 810016, China

[2]Xining Engineering Machinery Section, China Railway Qinghai-Xizang Group Co., Ltd, Xining 810016, China

[*]**Corresponding author:** Bing Guo, guobingsdu@qq.com

CITATION

Guan CY, Ma XJ & Guo B. The propeller design of a grazing drone based on MATLAB and XFOIL to select the optimal foil cross-section airfoil. Advanced Engineering & Precision Manufacturing. 2026; Vol 2(No. 1): 277.

https://doi.org/10.63808/aepm.v2i1.277

ARTICLE INFO

Received: 1 December 2025
Accepted: 9 December 2025
Available online: 8 March 2026

Abstract: In order to improve the flight efficiency of the grazing drone, the plateau grazing drone's propeller was designed using the Betz theory, and the airfoil selection method was improved in the design iteration process. The results show that the efficiency of the propeller designed by a single airfoil is 68.9%. The propeller's efficiency by selecting the optimal airfoil is 72.8%, which is improved by about 4%, and the design results are in good agreement with the CFD simulation results.

Keywords: Highland environment; Betz theory; High efficiency; Bézier fitting; MATLAB combined with XFOIL

1. Introduction

The Qinghai–Tibet Plateau is characterized by extremely low atmospheric pressure and air density, which significantly reduce the aerodynamic performance of

UAV propellers. In such low-Reynolds-number conditions, propellers are more prone to stall, especially at high pitch settings, leading to reduced lift, lower propulsive efficiency, and increased control load. These challenges make it essential to improve the aerodynamic design of propellers for high-altitude applications. To address these issues, more precise airfoil selection and optimization are required to ensure sufficient lift and efficiency under low-density conditions. This study focuses on the aerodynamic optimization of propeller airfoils suitable for high-altitude environments, with the goal of enhancing overall propeller performance and extending UAV endurance.

The design of the propeller is primarily based on Blade-element theory, which involves aerodynamic analysis of different cross-sections of the propellers. Both domestically and internationally, scholars have conducted extensive research on this topic, leading to a relatively mature theoretical foundation. In the early 20th century, in 1919, scientist Betz (1919) proposed a comprehensive theoretical framework for propeller design known as the minimum energy loss theory, which is also referred to as Betz's theory. This laid a solid theoretical basis for subsequent scientists studying the aerodynamic performance of propellers. Goldstein (1929) applied vortex theory, analogous to Blade-element theory, to approximate the flow characteristics of propellers by treating them as a system of bound vortices, examining ways to minimize energy losses generated during operation, and exploring approximate solutions for the no-vortex motion of propeller surfaces in Prandtl's inviscid fluid model. Larrabee (1979) proposed a comprehensive method for optimizing propeller design to minimize induced losses through lift line theory, induced velocity analysis, geometric optimization, and experimental validation. Eppler and Hepperle (1984) employed a reverse design method to optimize propeller design procedures, establishing target performance metrics and utilizing inverse computation techniques to determine the optimal propeller geometry and aerodynamic parameters to achieve the desired aerodynamic performance and efficiency. Adkins (1994) utilized a comprehensive approach combining aerodynamic theory, optimization algorithms, and experimental validation to design optimal propellers. Angelo et al. (2002) optimized propeller performance using a parametric design method, analyzing the impact of key design parameters on aerodynamic efficiency and employing optimization algorithms to adjust these parameters, thereby achieving optimal propeller design and performance. Burger and Hartfield (2007) developed a propeller

design methodology to maintain constant torque output, integrating detailed experimental testing and optimization techniques to ensure efficient performance and stability of the propeller under various operating conditions. Prior (2024) combined fundamental fluid dynamics principles with computational modeling to adjust the geometric parameters of propellers, resulting in optimal propeller design performance. Sapit et al. (2021) analyzes the aerodynamic characteristics of drone propellers using Computational Fluid Dynamics (CFD) to assess their performance under various operating conditions, aiming to provide recommendations for design improvements. Jain (2024) examines the thrust performance of various drone propeller designs through Computational Fluid Dynamics (CFD) simulations, aiming to identify optimal configurations that enhance efficiency and overall drone performance.

Although propeller design has advanced considerably, most existing methods use a single airfoil for all blade sections, limiting optimization and slowing iteration. This study addresses this by selecting optimal airfoils for each blade element based on local Reynolds and Mach numbers. A MATLAB-based iterative design approach integrates minimum energy loss theory with XFOIL aerodynamic calculations, while a CATIA interface using macros enables rapid modeling, significantly improving design efficiency.

2. Designing propellers based on the principle of minimum energy loss.

As shown in **Figure 1**, the process of designing propellers according to the principle of minimum energy loss is as follows (Betz, 1919):

Figure 1

Triangle of r-th Blade-element

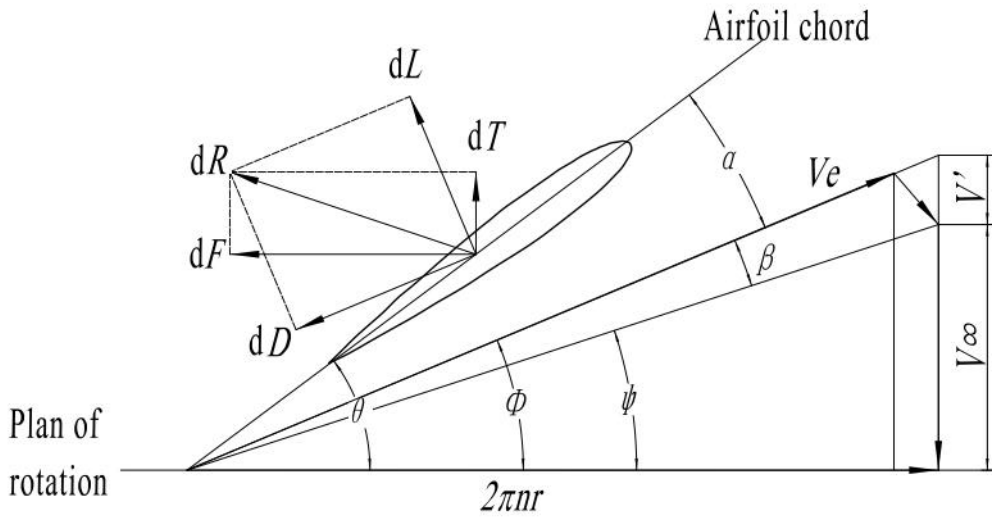

As illustrated in the blade element triangle, θ represents the pitch angle, Φ represents the actual flow angle, β represents the induced angle of attack, α represents the angle of attack, V_∞ represents the axial inflow velocity, and Ve represents the actual inflow velocity.

(1) Determine the number of selected stations for the propeller, identify the radius ri at each designated section, and design the chord length and pitch angle at each station.

(2) Calculate the Lagrange multiplier K.

$$\frac{T}{4\pi\rho V^2}=\int_{Rh}^{R}(K_1+K_1^2)k_p\mathrm{rdr} \tag{1}$$

$$k_p=\frac{2}{\pi}arccos\left(e^{-\frac{N}{2}(1-\frac{1}{R})\sqrt{1+(\frac{\Omega R}{V})^2}}\right) \tag{2}$$

$$K_1=\frac{K}{1+(\frac{V}{\Omega r})^2(1+K^2)} \tag{3}$$

where N represents the number of blades, R represents the propeller radius, T represents the required thrust, R_h represents the hub radius, and r represents the radius at the blade element station.

(3) Calculate the flow angle at the r-th blade element section.

$$\delta=arctan\left[\frac{\lambda}{\xi_i}(1+k)\right] \tag{4}$$

where $\lambda=\frac{V}{\Omega R}$ represents the forward ratio; $\xi_i=\frac{V_i}{R}$, represents the dimensionless radius at the r_i-th section.

(4) Calculate the chord length and pitch angle at section r_i.

Calculate the induced angle of attack:

$$\beta = \arctan\left(\frac{K\sin\delta\cos\delta}{1+K\cos^2\delta}\right) \tag{5}$$

Calculate the dimensionless flow velocity Ve':

$$Ve' = \sqrt{1+(\frac{\xi_i}{\lambda})^2} * \cos\beta \tag{6}$$

Calculate the local Reynolds number and Mach number:

$$Re_{\xi_i} = Ve' b * \mathrm{Re} \qquad Ma_{\xi_i} = Ve' * Ma \tag{7}$$

where b represents the dimensionless chord length, and $u=1.76\times10^{-5}$ represents the kinematic viscosity. $Re=\rho VR/\mu$ represents the free Reynolds number, $Ma=V/c$ represents the free Mach number.

(5) Perform iterative calculations for the dimensionless chord length.

The calculation formula for the dimensionless chord length is:

$$B = \frac{8\pi}{N}\frac{\xi_i k_p \tan\beta \sin\theta}{Cl\tan\theta max_{max}} \tag{8}$$

where Cl_{max} and Cd_{max} represent the maximum lift coefficient and maximum drag coefficient corresponding to the maximum lift-to-drag ratio within the angle of attack range, calculated during the iteration using XFOIL.

In this study, the dimensionless chord length allows for the calculation of local Mach and Reynolds numbers as described in Equation (7). Based on the local Mach and Reynolds numbers, XFOIL is used to iteratively derive the angle of attack α corresponding to the maximum lift-to-drag ratio. The parameter b is then gradually increased to determine the chord length corresponding to the minimum value of $|b-B|$. This approach yields the aerodynamic characteristics of the section, including the airfoil angle of attack and lift-to-drag coefficients. To prevent excessive chord lengths and angles of attack, constraints are applied such that the chord length remains below $0.2R$ and the angle of attack remains under 10°. This paper improves upon the iterative methods of Angelo et al. by fitting the chord length and pitch angle using Beizer curves to reduce the number of iterative sections. Additionally, the combination of Betz's theory and XFOIL in MATLAB enables continuous distribution of chord lengths, thereby accelerating the iteration speed.

Pitch angle:

$$\theta = \phi + \alpha \tag{9}$$

(6) Sequentially repeat the above calculation process for different stations to determine the distribution of chord lengths and pitch angles at each section.

(7) Calculate the efficiency of the propeller:

$$\zeta=\int_{\xi_1}^{1}\frac{N\lambda^2}{2}Ve'(Cl_{\max}\cos\phi-Cd_{\max}\sin\phi)bd\xi \tag{10}$$

$$\kappa=\int_{\xi_1}^{1}\frac{N\lambda^2}{2}Ve'(Cl_{\max}\sin\phi+Cd_{\max}\cos\phi)b\xi d\xi \tag{11}$$

$$\eta=\frac{\zeta\lambda}{\kappa} \tag{12}$$

3. Design of propellers for high-altitude herding applications.

3.1. Propeller design parameters.

For a small high-altitude herding drone operating at 2200 m (air density 0.9869 kg/m³), this study aims to design a cruise-optimized propeller to maximize aerodynamic efficiency. The drone uses a two-blade propeller and requires 8 N of cruise thrust; therefore, a design thrust of 10 N is adopted to ensure sufficient thrust margin. The design parameters include a rotational speed of 2500 r/min, a blade radius of 0.3 m, a hub radius of 0.02 m, and a cruise speed of 10 m/s. MATLAB is used to access the airfoil library, and the selected airfoils are analyzed in XFOIL to obtain aerodynamic characteristics. The optimal airfoils for each blade section are iteratively determined to maximize overall propeller efficiency. The design parameters of the propeller are shown in **Table 1**.

Table 1

Propeller parameters

PARAMETER	VALUE	UNIT
ROTATION SPEED *N*	2500	rpm
THRUST *T*	10	N
NUMBER OF BLADES *N*	2	
PROPELLER RADIUS *R*	0.3	m
HUB RADIUS *RH*	0.02	m
DENSITY *P*	0.9869	kg/m³
VELOCITY *V*	10	m/s

WISDOM ACADEMIC ISSN: 3105-1693 | E-ISSN: 3105-1707 Volume 2 , Issue 1

3.2. Design a single airfoil for the selected section.

First, the propeller is designed using the NACA 0012 airfoil, which demonstrates stable performance at low Reynolds numbers and is commonly used in small to medium-sized drones, as illustrated in **Figure 2**.

Figure 2

NACA 0012 airfoil

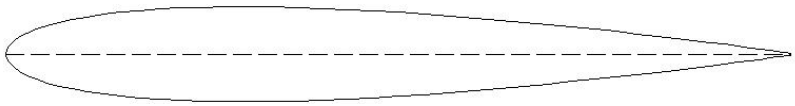

Based on Equations (1), (2), and (3), the Lagrange multiplier K is calculated to be 0.1988. Using Equations (10), (11), and (12), the efficiency is determined to be 68.9%.

3.3. Select the optimal airfoil for the section design.

The high-altitude pastoral environment is characterized by low air pressure and low air density, resulting in low-Reynolds-number operating conditions and reduced propeller lift. To avoid excessive computational cost from the large airfoil database, this study selects several airfoils with proven low-Reynolds-number adaptability. Such airfoils typically feature: (1) a relatively large thickness-to-chord ratio to delay flow separation and enhance lift; (2) an optimized, rounder leading edge to reduce the likelihood of separation; and (3) a thinner trailing edge to decrease separation and induced drag.

The selected airfoils include Eppler 387, Eppler 420, Clark Y, NASA 0614, NACA 6412, NACA 64-215, FX 63-137, and RAF 6, all of which offer favorable aerodynamic characteristics in low-Reynolds-number conditions. Additionally, NACA 0012 is included for comparison. These ten airfoils are evaluated to identify the optimal design. Using the method described in Section 2, the Lagrange multiplier K is obtained as 0.1988, and the resulting efficiency reaches 72.8%, representing an improvement of about 4% over the single-airfoil design baseline. The chord length and pitch angle distributions from the two design approaches are shown in **Figure 3**. The airfoil distribution of the propeller section is shown in **Table 2**.

Figure 3

Propeller design results

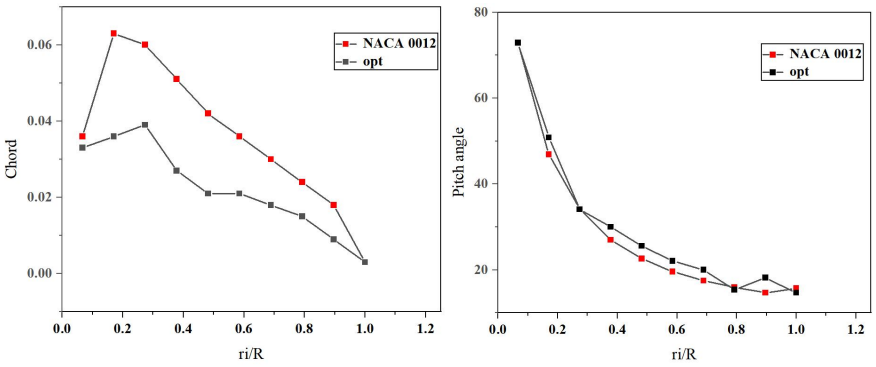

Table 2

Propeller parameters

r_i/R	0.0667	0.1704	0.2741	0.3778	0.4815	0.5852	0.6889	0.7926	0.8963	1
Airfoil	NASA 0614	Eppler 387	RAF 6	Eppler 387	Eppler 387	Eppler 387	Eppler 387	RAF 6	Eppler 387	Eppler 387

When comparing the optimized airfoils, the overall Reynolds number of the propeller is approximately 300000. A comparison was made between the selected optimal airfoils and the single airfoil NACA 0012 under this Reynolds number condition, as shown in **Figure 4**. The analysis indicates that the Eppler 387 airfoil exhibits a high lift-to-drag ratio at angles of attack between 3° and 5°. In comparison, the RAF 6 airfoil also demonstrates a high lift-to-drag ratio at angles of attack from 5° to 10°. In contrast, the NACA 0012 airfoil has a higher torque coefficient, resulting in more significant drag and a comparatively lower lift-to-drag ratio. Therefore, when designing airfoils based on the principle of minimum energy loss, the Eppler 387 and RAF 6 airfoils will be prioritized.

Figure 4

Different airfoil lift-to-drag ratios and moment coefficients at different angles of attack with a Reynolds number of 300,000

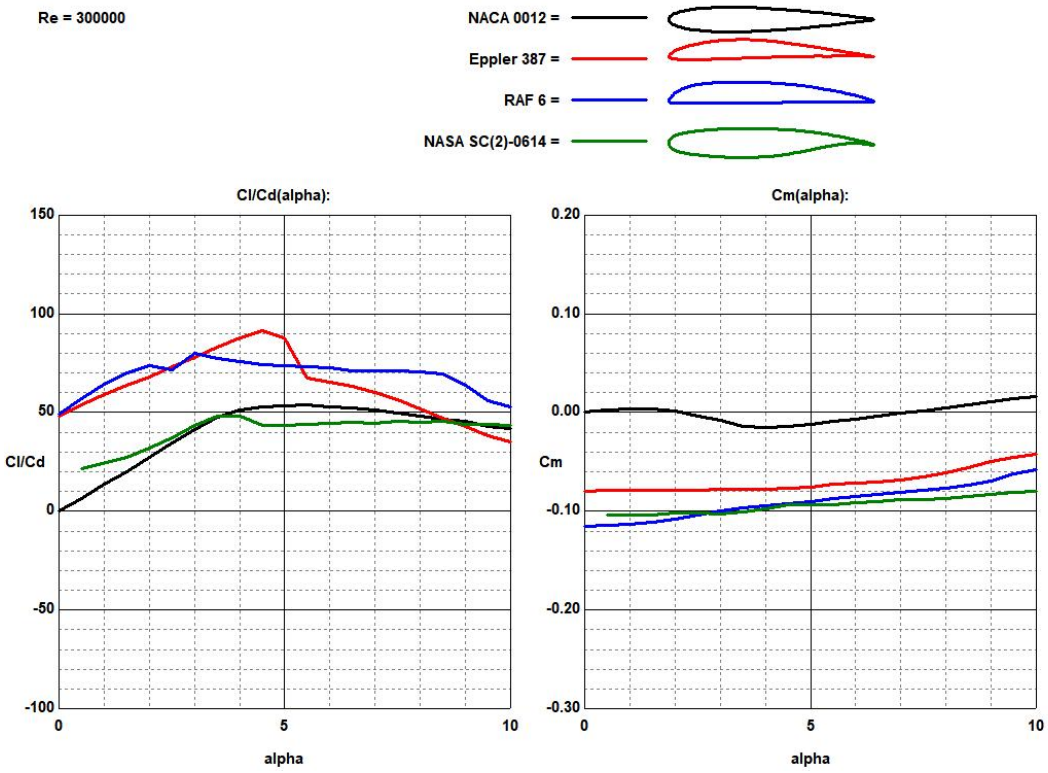

3.4. Fitted chord length and pitch angle

This study reduces the number of design sections and computational time by using Bézier curves for fitting, resulting in the design of 10 sections. The fitted chord lengths and pitch angles ensure smoothness and continuity in their distribution. The fitting results of the chord length and pitch Angle are shown in **Figure 5**.

$$B(t)=\sum_{i=0}^{n}\binom{n}{i}P_i(1-t)^{n-i}t^i=\binom{n}{0}P_0(1-t)^n t^0+\binom{n}{1}P_1(1-t)^{n-1}t^1+\ldots$$

$$+\binom{n}{n_i}P_{n_i}(1-t)^{n-n_i}t^{n_i-1}+\binom{n}{n}P_n(1-t)^0 t^n, t\in[0,1] \quad (13)$$

Figure 5

Bézier fitting results

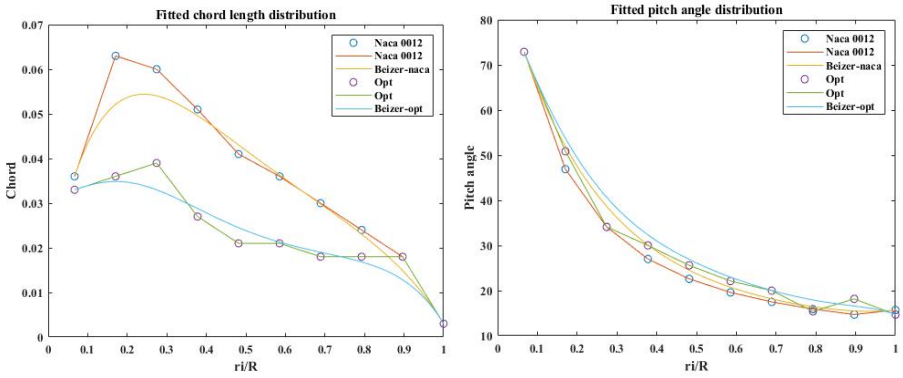

The MSE analysis of the fitting results indicates that all values are below 0.02, meeting the required accuracy.

$$MSE=\frac{1}{n}\sum_{i=1}^{n}(y_i-\hat{y}_i)^2 \tag{14}$$

where n is the total number of data points, y_i is the actual value, and $\hat{y}_i$ is the fitted value.

4. Numerical simulation validation

4.1. Aerodynamic Analysis Method

4.1.1 Mathematical model

The model adheres to the fundamental laws of fluid mechanics, using the Navier-Stokes equations as the governing equations. It follows the principle of mass conservation: the increase in mass within a fluid element over a unit of time is equal to the net mass flowing into that element during the same period.

$$\frac{\partial\rho}{\partial t}+\frac{\partial(\rho u)}{\partial x}+\frac{\partial(\rho v)}{\partial y}+\frac{\partial(\rho w)}{\partial z}=0 \tag{15}$$

where ρ represents the turbulent air density; u represents the velocity in the x-direction; v represents the velocity in the y-direction; and w represents the velocity in the z-direction.

The model also complies with the momentum conservation equation: the momentum change rate within the fluid element concerning time is equal to the sum of all external forces acting on that element.

$$x\text{direction:}\frac{\partial(\rho u)}{\partial t}+div(\rho uu)=-\frac{\partial\rho}{\partial x}+\frac{\partial\tau_{xx}}{\partial x}+\frac{\partial\tau_{xy}}{\partial y}+\frac{\partial\tau_{xz}}{\partial z}+F_x \tag{16}$$

$$y\text{direction:}\frac{\partial(\rho v)}{\partial t}+div(\rho vu)=-\frac{\partial\rho}{\partial y}+\frac{\partial\tau_{xy}}{\partial x}+\frac{\partial\tau_{yy}}{\partial y}+\frac{\partial\tau_{zy}}{\partial z}+F_y \tag{17}$$

$$z\text{direction:}\frac{\partial(\rho w)}{\partial t}+div(\rho wu)=-\frac{\partial\rho}{\partial z}+\frac{\partial\tau_{xz}}{\partial x}+\frac{\partial\tau_{yz}}{\partial y}+\frac{\partial\tau_{zz}}{\partial z}+F_z \tag{18}$$

where ρ represents the fluid density; τ represents the shear stress on the surface, where the first subscript indicates that the stress component acts on a surface perpendicular to the x-axis, and the second subscript indicates the direction of the stress component, which can be x, y, or z.

4.1.2 Fluid computational model.

This study employs the Realizable k-epsilon turbulence model with rotational corrections for simulation. Compared to the standard k-epsilon model and the RNG k-epsilon model, the Realizable k-epsilon model introduces an additional viscosity formula that effectively addresses complex flow fields involving curvature, vortices, and rotation, thereby enhancing the accuracy of the simulations.

$$\frac{\partial(\rho k)}{\partial t}+\frac{\partial(\rho k u_j)}{\partial x_i}=\frac{\partial[(\mu+\frac{\mu_i}{\partial k})\frac{\partial k}{\partial x_j}]}{\partial x_i}+G_k+G_b-\rho\in-Y_M+S_k \quad (19)$$

$$\frac{\partial(\rho\Xi)}{\partial t}+\frac{\partial(\rho\Xi u_j)}{\partial x_j}=\frac{\partial\left[\left(\mu+\frac{\mu_t}{\sigma_\varepsilon}\right)\frac{\partial\Xi}{\partial x_j}\right]}{\partial x_j}+\rho C_{1\varepsilon}S_\varepsilon-\rho C_{2\varepsilon}\frac{\Xi^2}{k+\sqrt{v\Xi}}+C_{1\varepsilon}\frac{\Xi}{k}C_{2\varepsilon}G_\varepsilon+S_\varepsilon \quad (20)$$

$$C_1=max\left[0.43,\frac{\eta}{\eta+5}\right]$$

$$\eta=S\frac{k}{\in} \quad (21)$$

where G_k represents the turbulence kinetic energy generated by the shear gradient, G_b represents the turbulence kinetic energy generated by buoyancy, and C_1, C_2, and ϵ are constants. σ_k and σ_e represent the turbulence Prandtl numbers in the k and epsilon equations, respectively.

4.2. Grid Generation and Boundary Condition Setup

A three-dimensional model of the optimized propeller based on the selected airfoil sections is created, as shown in **Figure 6**.

Figure 6

Three-dimensional model of propeller

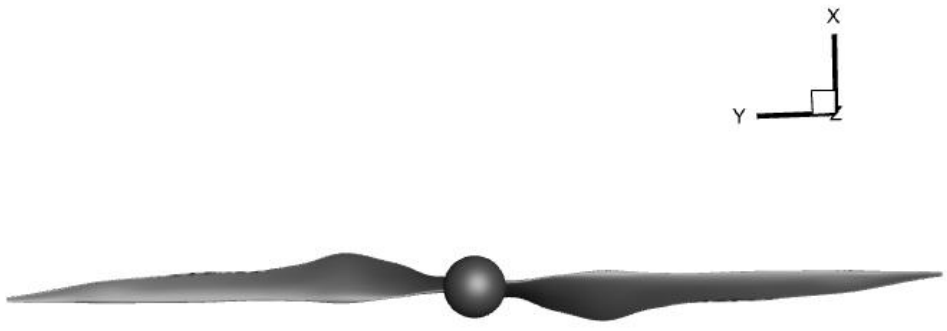

The computational domain is divided into two parts: a stationary domain and a rotating domain, as shown in **Figure 7**. After the blade element section optimization,

the propeller is meshed using Ansys Meshing. A tetrahedral unstructured mesh is employed, which captures the airfoil curvature well. A 5-layer boundary layer mesh also captures the airflow characteristics near the wall. The total number of mesh elements is 4498584; the minimum orthogonal quality of the mesh is 0.11, and the mesh quality is appropriate. The distribution of local mesh elements is illustrated in **Figure 8**.

Figure 7

Schematic of the Computational Domain

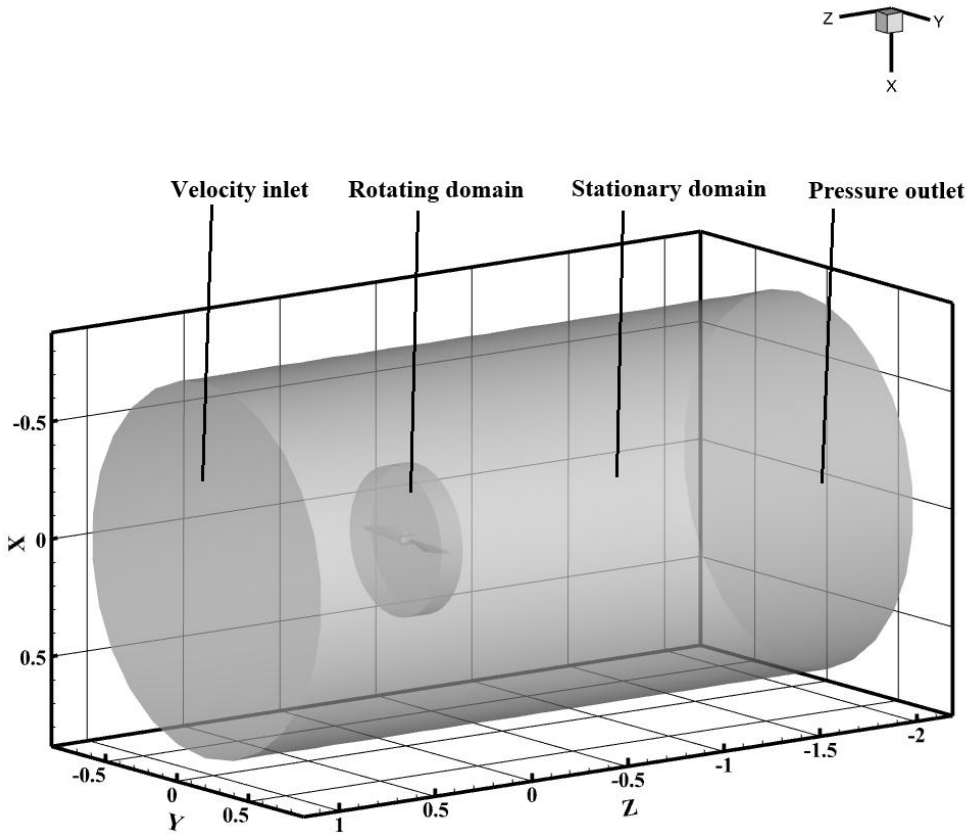

Figure 8

Schematic diagram of the local grid

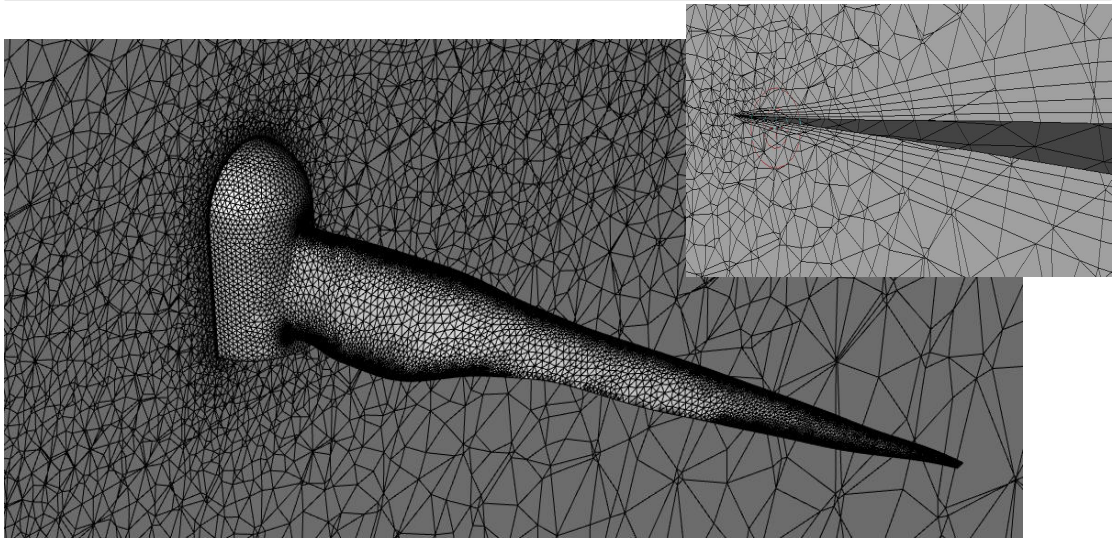

The MRF approach is used to model propeller rotation. A 10 m/s velocity inlet represents cruise conditions, and a pressure outlet is applied downstream. Zero-shear far-field boundaries simulate an unbounded external flow. At 2200 m altitude, the ambient pressure is 77,406 Pa and the air density is 0.9869 kg/m³. A coupled solver is employed, using first-order upwind discretization for turbulence variables and second-order upwind for momentum. Boundary conditions are listed in **Table 3**.

Table 3

Boundary condition parameters

Density	Pressure	Inlet	Outlet	Method
0.9869kg/m³	77406pa	Velocity inlet （10m/s）	Pressure outlet	Couple

4.3. Numerical simulation results

Figure 9 presents the numerically predicted efficiency and thrust at different rotational speeds. Thrust increases with rotational speed, and the results remain consistent with the CFD predictions, particularly at higher speeds, indicating reliable aerodynamic performance. The power curve first rises and then falls, with a peak efficiency of 0.729 at the design speed—only 0.001 higher than the design value of 0.728—demonstrating excellent accuracy. Although the efficiency reaches 0.833 at 2300 r/min, the corresponding thrust fails to meet the design requirement.

Figure 9

CFD simulation results: (a) Variation curve of lift with rotational speed (V=10m/s); (b) Variation curve of CFD Efficiency with rotational speed (V=10m/s)

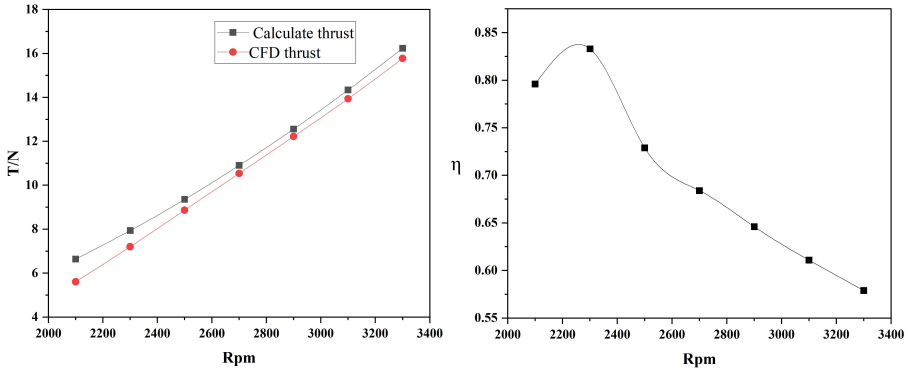

(a) (b)

5. Conclusion

Based on the principle of minimum energy loss, this study implemented a joint iteration of the minimum energy design theory with the aerodynamic analysis software XFOIL using MATLAB. This optimization focused on selecting airfoils for different blade sections in propeller design. Using MATLAB and XFOIL, various airfoils suitable for low Reynolds numbers were chosen for different radial positions, resulting in efficient chord length and pitch angle distributions for a high-altitude grazing drone propeller. The feasibility and accuracy of the design were validated through CFD numerical simulations. The main conclusions drawn are as follows:

1) Using the principle of minimum energy loss allows for the design of practical and highly accurate propellers.

2) By employing Bézier curve fitting for chord length and pitch angle and integrating Betz's theory with XFOIL in MATLAB for joint iteration, the design computation workload and time can be significantly reduced.

3) By utilizing MATLAB in conjunction with XFOIL to select optimal airfoils from the airfoil library for different radial sections, the propeller's aerodynamic performance and efficiency can be significantly enhanced compared to single airfoil designs.

4) The CFD numerical simulation results align closely with the design values, demonstrating that this method can significantly reduce the costs and time required for wind tunnel experiments, thus enhancing design efficiency.

Conflict of interest: The authors declare no conflict of interest.

Funding: This research received no external funding.

References

[1] Adkins, C. N., & Liebeck, R. H. (1994). Design of optimum propellers. *Journal of Propulsion and Power, 10*(5), 676–682.

[2] Betz, A. (1919). *Airscrews with minimum energy loss* (Report No. 15). Kaiser Wilhelm Institute for Flow Research. -1-4-10

[3] Burger, C., & Hartfield, R. (2007). Design, testing and optimization of a constant torque propeller [Paper presentation]. 25th AIAA Applied Aerodynamics Conference, Miami, FL, United States. (Article 3927)

[4] D'Angelo, S., Berardi, F., & Minisci, E. (2002). Aerodynamic performances of propellers with parametric considerations on the optimal design. *The Aeronautical Journal, 106*(1060), 313–320.

[5] Eppler, R., & Hepperle, M. (1984). A procedure for propeller design by inverse methods. In *Proceedings of the International Conference on Inverse Design Concepts in Engineering Sciences (ICIDES)* (pp. 445–460). Austin, TX, United States.

[6] Goldstein, S. (1929). On the vortex theory of screw propellers. *Proceedings of the Royal Society of London. Series A, Containing Papers of a Mathematical and Physical Character, 123*(792), 440–465. -2-7

[7] Jain, D., & Vishwakarma, V. (2024). Investigation of thrust performance for different drone propeller designs using CFD. In *Opportunities and risks in AI for business development: Volume 1* (pp. 299–310). Springer Nature. https://doi.org/10.1007/978-3-031-65203-5_27-3

[8] Larrabee, E. E. (1979). Practical design of minimum induced loss propellers. *SAE Transactions, 88*, 2053–2062.

[9] Prior, S. D., & Newman-Sanders, D. (2024). Advanced scale-propeller design using a MATLAB optimization code. *Applied Sciences, 14*(14), 6296.

[10] Sapit, A., Masjan, M. F., & Shater, S. K. (2021). Aerodynamics drone propeller analysis by using computational fluid dynamics. *Journal of Complex Flow, 3*(2), 12–16.